

Supporting Information

Aggregation Effects on Photophysical Properties of NBN-Doped Polycyclic Aromatic Hydrocarbons: A Theoretical Study

Yi Zeng,^a Junfang Yang^a and Xiaoyan Zheng^{a,b,*}

^aKey Laboratory of Cluster Science of Ministry of Education, Beijing Key laboratory of Photoelectronic/Electro-photonic Conversion Materials, School of Chemistry and Chemical Engineering, Beijing Institute of Technology, Beijing, 100081, China.

^bGuangdong Provincial Key Laboratory of Luminescence from Molecular Aggregates (South China University of Technology), Guangzhou 510640, China.

List of Contents

I. Computational details

- 1.1 Nucleus independent chemical shifts (NICS) calculation.
- 1.2 Anisotropy of induced current density (ACID) calculation.
- 1.3 Visualization of shielding tensors (VIST) method.

II. Supplementary Figures S1-S13

Fig. S1 (a) The PCM model of NBN-6 in dilute methanol solution. (b) The amorphous aggregate of NBN-5 extracted from the MD simulations. The embedded QM/MM model (top) and exposed QM/MM model (bottom) for NBN-5 embedded in amorphous aggregate or exposed on its surface. (c) The QM/MM model of NBN-5 in the crystalline state. Each QM/MM model was set up by choosing one NBN-5 molecule as the QM region and the others as the MM region, respectively.

Fig. S2 Chemical Structures of two representative NBN-doped PAHs: six-membered NBN-6 and five-membered NBN-5. The key structural parameters and the index of key atoms were labeled, respectively.

Fig. S3 The possible resonance structural formulas of NBN-6 and NBN-5 respectively.

Fig. S4 (a) The NICS(1) values of rings A, B and C at T₁ state. (b) The visualization of chemical shielding tensors for the T₁ states of NBN-6 and NBN-5 computed 1 Å above the A, B, C rings (the NICS(1) value is a third of the sum of the three eigenvalues at x, y, z direction). (c) The ACID plots of NBN-6 and NBN-5 at T₁ state.

Fig. S5 The electron density contours of HOMO and LUMO at S₁ geometry for both (a) NBN-6 and (b) NBN-5 in methanol solution.

Fig. S6 The electron density contours of HOMO and LUMO for both (a) NBN-6 and (b) NBN-5 in crystalline states.

Fig. S7 Detailed information of fragments A and B of NBN-5 and NBN-6, as well as the properties of their transition orbitals.

Fig. S8 The HOMO, LUMO energy level and energy gaps of both (a) NBN-6 and (b) NBN-5 at S₀ state.

Fig. S9 Transition dipole moments of (a) NBN-6 and (b) NBN-5 at S₁ geometries of the exposed and crystalline phase. (units: Debye)

Fig. S10 Reorganization energy vs normal mode frequency of S₁ state of three representative embedded NBN-6 molecules in amorphous aggregates.

Fig. S11 Reorganization energy vs normal mode at S₁ state of NBN-5 molecules at different environments.

Fig. S12 The molecular packing in crystal along different directions of (a) NBN-6 and (b) NBN-5.

Fig. S13 The molecular packing around the selected QM molecule of (a) NBN-6 and (b) NBN-5 extracted from the amorphous aggregates.

III. Supplementary Tables S1-S12

Table S1. The calculated absorption and emission wavelength, as well as excitation energies of NBN-6 and NBN-5 in methanol solution by PCM model using several different functionals with basis set 6-31+G(d,p), respectively.

Table S2. Selected structural parameters of NBN-6 at different environments (including solution, one exposed and four embedded molecule of amorphous aggregates, crystal) at both S₀ and S₁ minimum, respectively.

Table S3. Selected structural parameters of NBN-5 at different environments (including solution, one exposed and four embedded molecule of amorphous aggregates, crystal) at both S₀ and S₁ minimum, respectively.

Table S4. The calculated NICS(1) values of ring A, B and C in NBN-6 and NBN-5 at S_0 and T_1 states.

Table S5. Calculated vertical excitation energy (ΔE_{vert}), EDM, f and the transition orbitals assignment of NBN-6 and NBN-5 at the different phases.

Table S6. Contributions of heavy atoms in rings B and C to HOMO and LUMO of both NBN-6 and NBN-5.

Table S7. Calculated k_r , k_{ic} and fluorescent quantum efficiency (FQE) of both NBN-6 and NBN-5 at different environments (including methanol solution, exposed and embedded molecules in amorphous aggregates and crystals).

Table S8. Reorganization energies of NBN-6 and NBN-5 obtained by both the adiabatic potential energy surface (AP) and normal mode analysis (NM) methods in the different phases.

Table S9. The projected reorganization energies of six representative normal modes of NBN-6 at different environments.

Table S10. The excitonic coupling constants (J) of pairwise dimers (shown in Fig. S11) extracted from the crystal structures of NBN-6 and NBN-5.

Table S11. The excitonic coupling constants (J) of pairwise dimers (shown in Fig. S12) extracted from the amorphous aggregates of NBN-6 and NBN-5.

Table S12. Intermolecular distances for the dimer with the maximum excitonic coupling constants (J) at different environments and the corresponding ratios J/λ_{gs} and J/λ_{es} of NBN-6 and NBN-5.

IV. References

I. Computational details

1.1 Nucleus independent chemical shifts (NICS) calculation.

The nucleus independent chemical shifts (NICS)^{1, 2} of NBN-6 and NBN-5 at S₀/T₁ states perpendicular to the ring-plane at 1 Å off the ring-center (NICS(1)^{3, 4}) of ring A, B and C were calculated at MPW1LYP^{5, 6}/6-31+G(d,p) level with gauge invariant atomic orbital (GIAO) approach⁷⁻¹⁰ using Gaussian 16 program.¹¹ The calculated NICS value at S₀/T₁ states are based on the optimal structures of S₀/T₁ states respectively.

1.2 Anisotropy of induced current density (ACID) calculation.

The anisotropy of induced current density (ACID) calculation¹² were performed to analyze the ring-currents at S₀/T₁ states of NBN-6 and NBN-5 systems through the continuous set of gauge transformations (CSGT) methodology^{13, 14} at MPW1LYP^{5, 6}/6-31+G(d,p) level. The optimized geometries at S₀/T₁ states were used to analyze the ACID and the results were visualized by the POV-Ray 3.7.

1.3 Visualization of shielding tensors (VIST) method.

The shielding tensors at different direction based on the value of NICS at S₀/T₁ states were analyzed by the VIST method implemented by TheoDORE wavefunction analysis package.¹⁵⁻¹⁷ The graphs of the tensor representations in connection with molecular structures were plotted by the visual molecular dynamics (VMD) program.¹⁸

II. Supplementary Figures

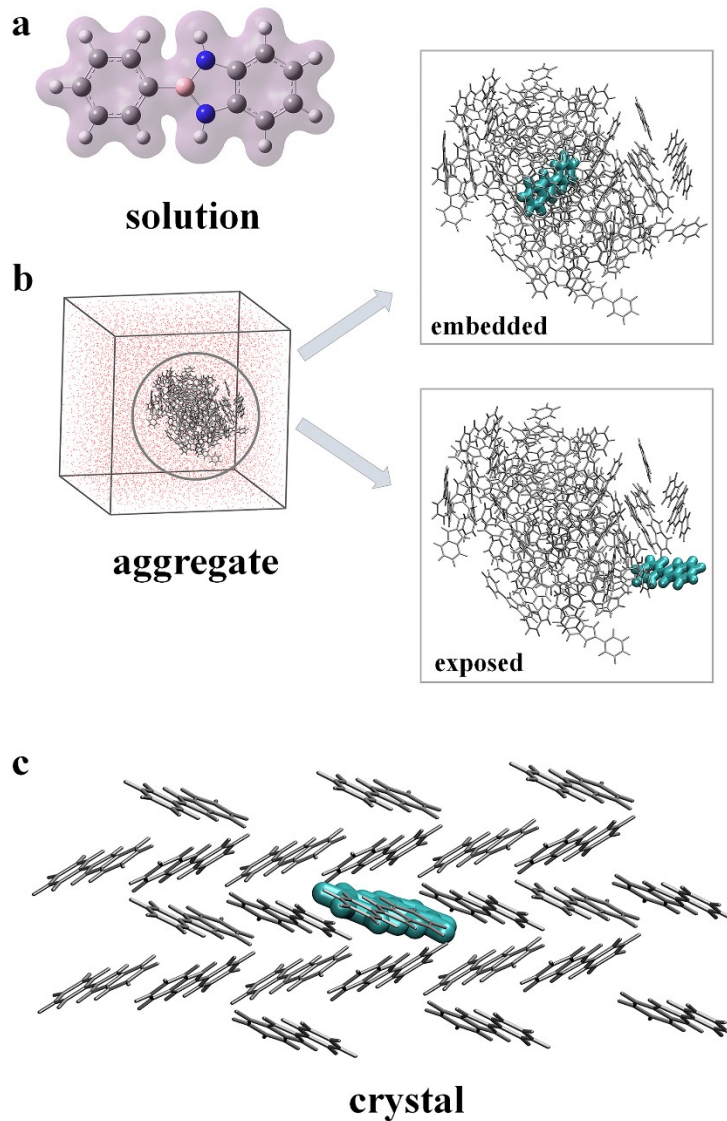


Fig. S1 (a) The PCM model of NBN-6 in dilute methanol solution. (b) The amorphous aggregate of NBN-5 extracted from the MD simulations. The embedded QM/MM model (top) and exposed QM/MM model (bottom) for NBN-5 embedded in amorphous aggregate or exposed on its surface. (c) The QM/MM model of NBN-5 in the crystalline state. Each QM/MM model was set up by choosing one NBN-5 molecule as the QM region and the others as the MM region, respectively.

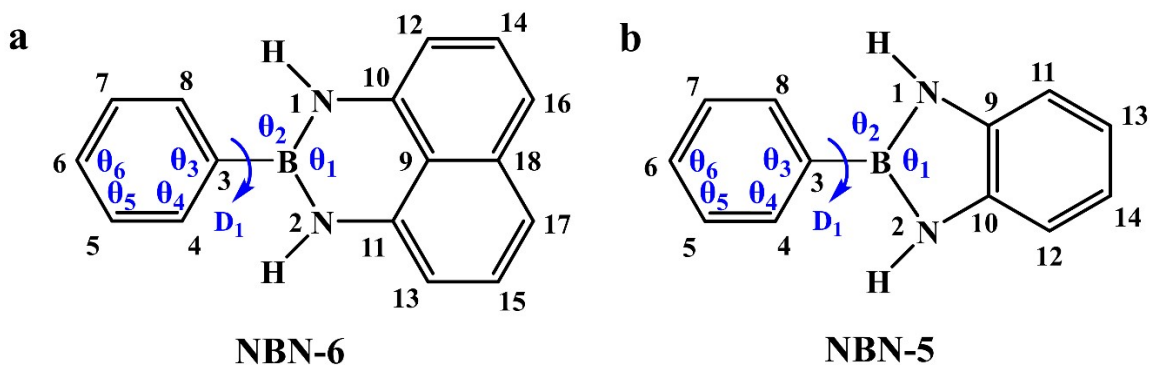


Fig. S2 Chemical Structures of two representative NBN-doped PAHs: six-membered NBN-6 and five-membered NBN-5. The key structural parameters and the index of key atoms were labeled, respectively.

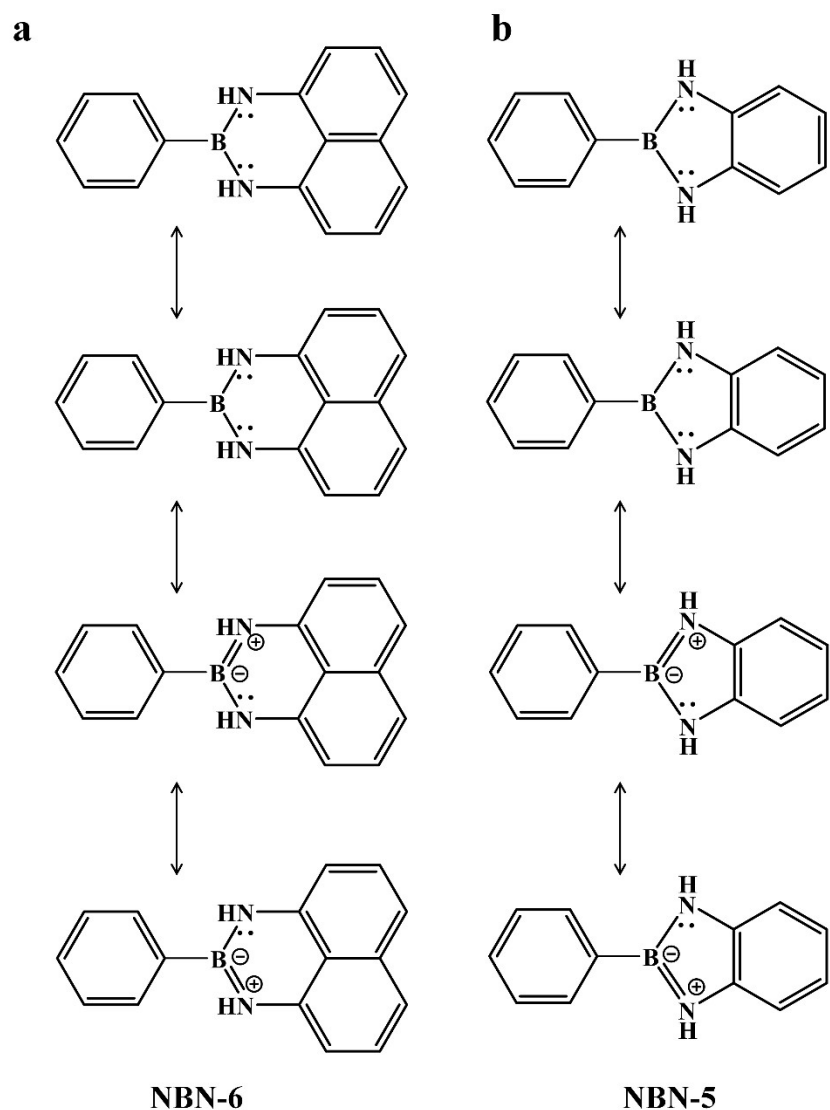


Fig. S3 The possible resonance structural formulas of NBN-6 and NBN-5 respectively.

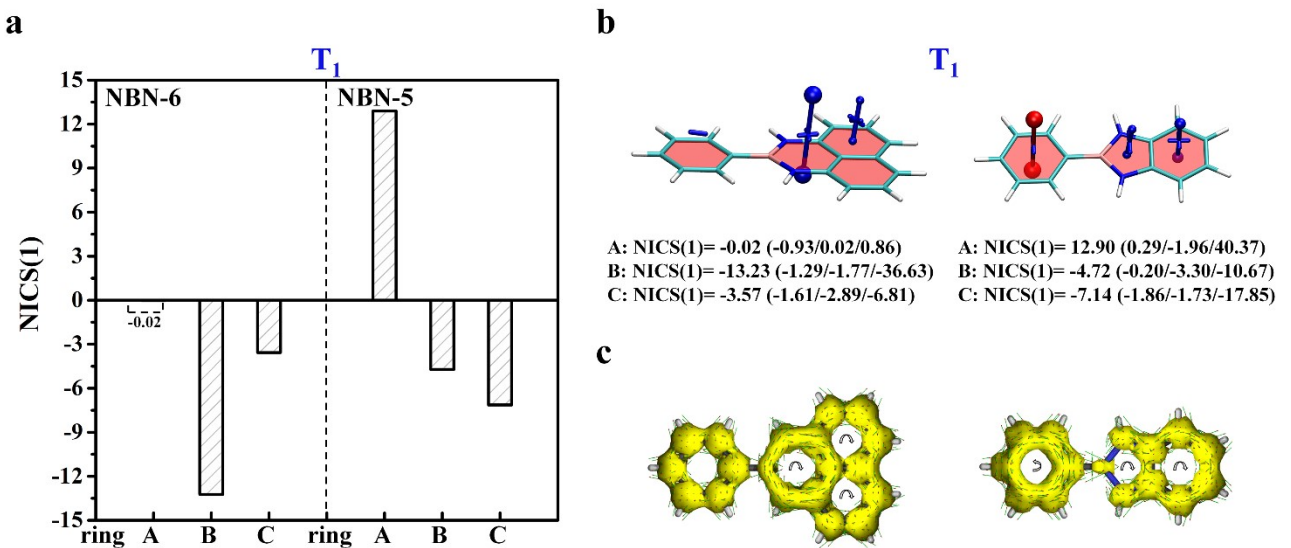


Fig. S4 (a) The NICS(1) values of rings A, B and C at T_1 state. (b) The visualisation of chemical shielding tensors for the T_1 states of NBN-6 and NBN-5 computed 1 Å above the A, B, C rings (the NICS(1) value is a third of the sum of the three eigenvalues at x, y, z direction). (c) The ACID plots of NBN-6 and NBN-5 at T_1 state.

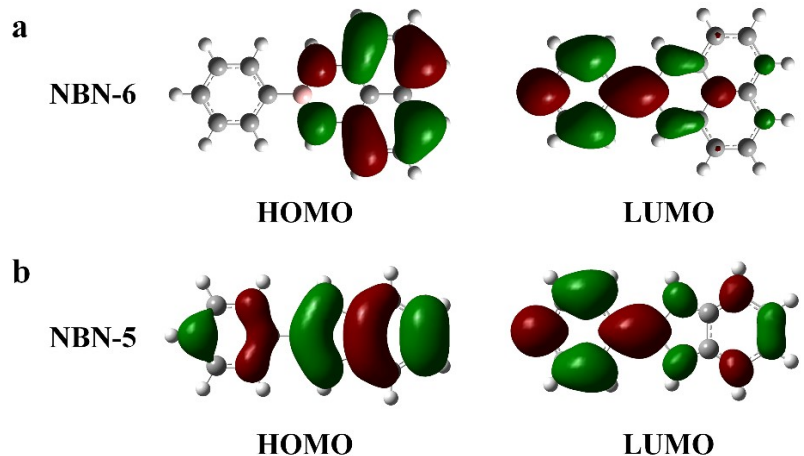


Fig. S5 The electron density contours of HOMO and LUMO at S_1 geometry for both (a) NBN-6 and (b) NBN-5 in methanol solution.

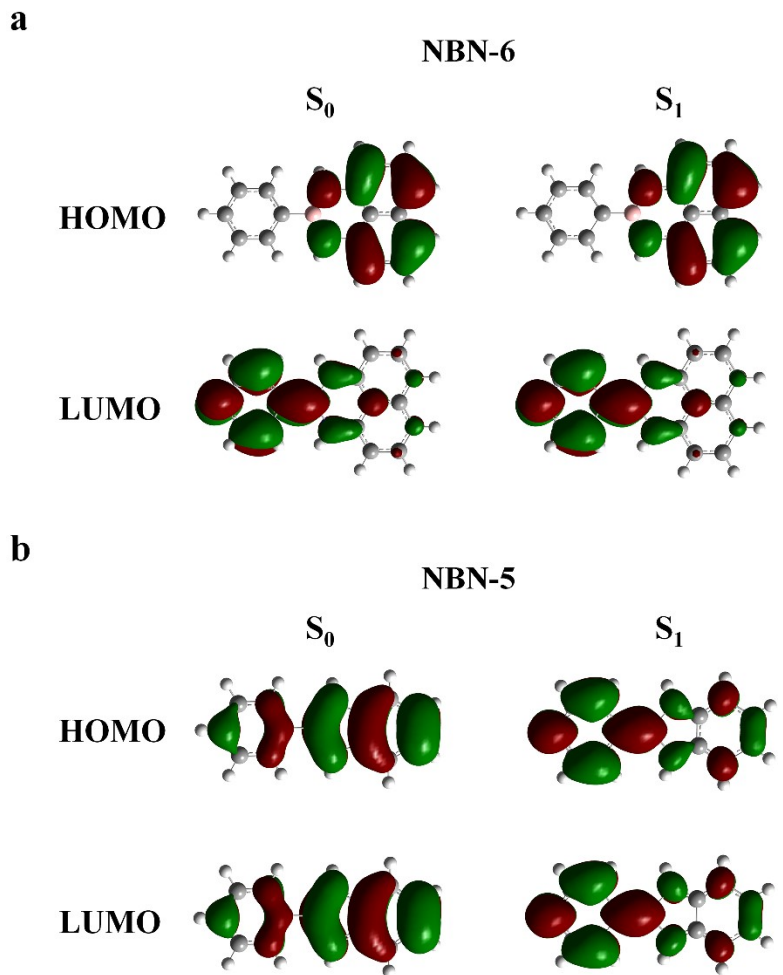


Fig. S6 The electron density contours of HOMO and LUMO for both (a) NBN-6 and (b) NBN-5 in crystalline states.

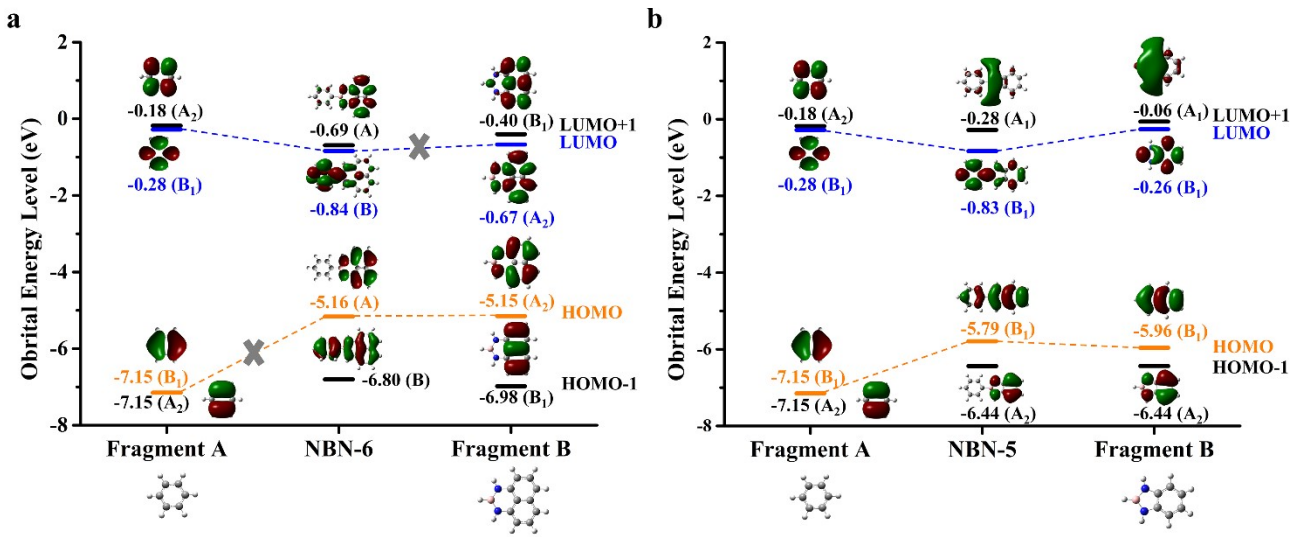


Fig. S7 Detailed information of fragments A and B of NBN-5 and NBN-6, as well as the properties of their transition orbitals.

The transition between S_0 and S_1 of both NBN-6 and NBN-5 are dominated by HOMO \rightarrow LUMO with assignments surpass 90% and 96%, respectively. It is found that both NBN-5 and NBN-6 consist of two conjugated fragments A and B connected by a single bond (Fig. S7). As shown in Fig. S7, the HOMO of NBN-5 is obtained by combining HOMO of fragments A and B, in the meanwhile the LUMO of NBN-5 also combined by the corresponding LUMO of two fragments, because of the consistent molecular orbital symmetry B_1 . For NBN-6, the symmetry of HOMO or LUMO of two fragments are different, therefore, the HOMO of NBN-6 was mainly contributed by fragment B, and LUMO was mainly contributed by fragment A. Therefore, the HOMO and LUMO of NBN-5 delocalized on the entire backbone, while the HOMO and LUMO of NBN-6 were localized on fragment B and A, respectively. The different distribution and symmetry of transition orbitals of NBN-5 and NBN-6 lead to different transition dipole moments. Therefore, the S_1 state is polarized along the long molecular axis for NBN-5 but perpendicular to it for NBN-6.

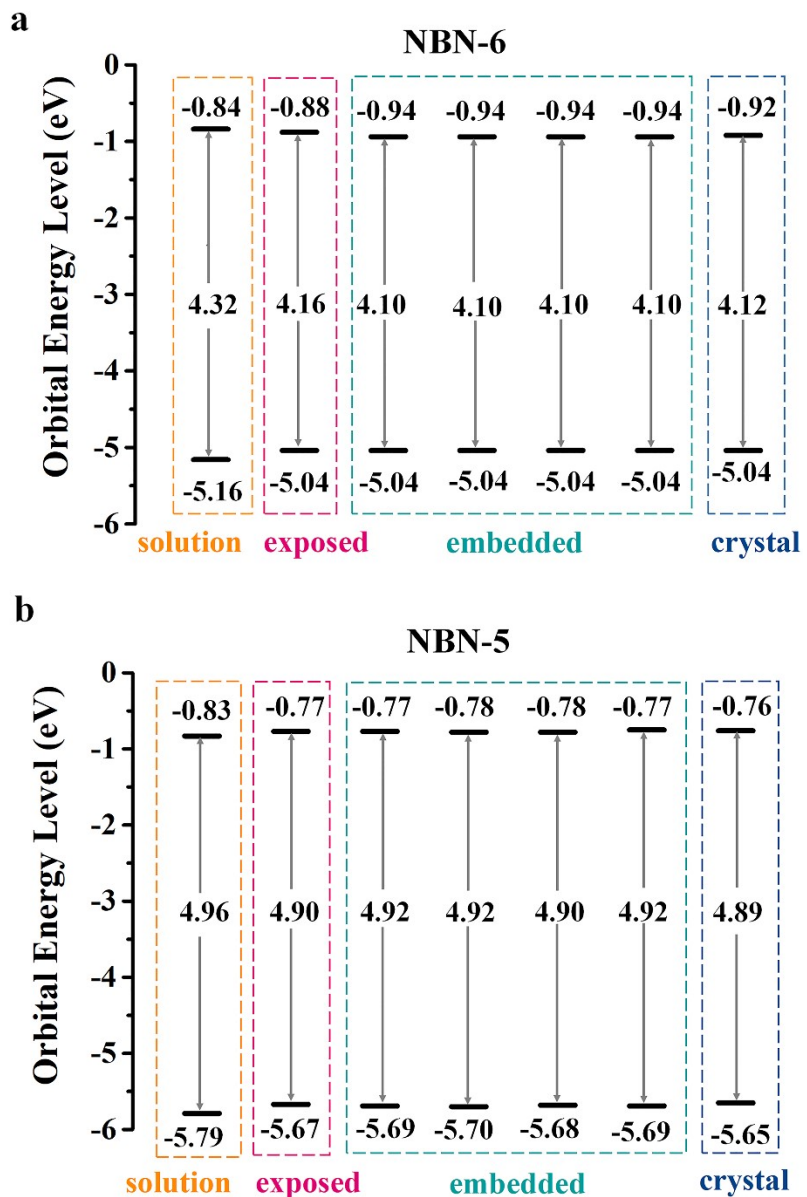


Fig. S8 The HOMO, LUMO energy level and energy gaps of both (a) NBN-6 and (b) NBN-5 at S_0 state.

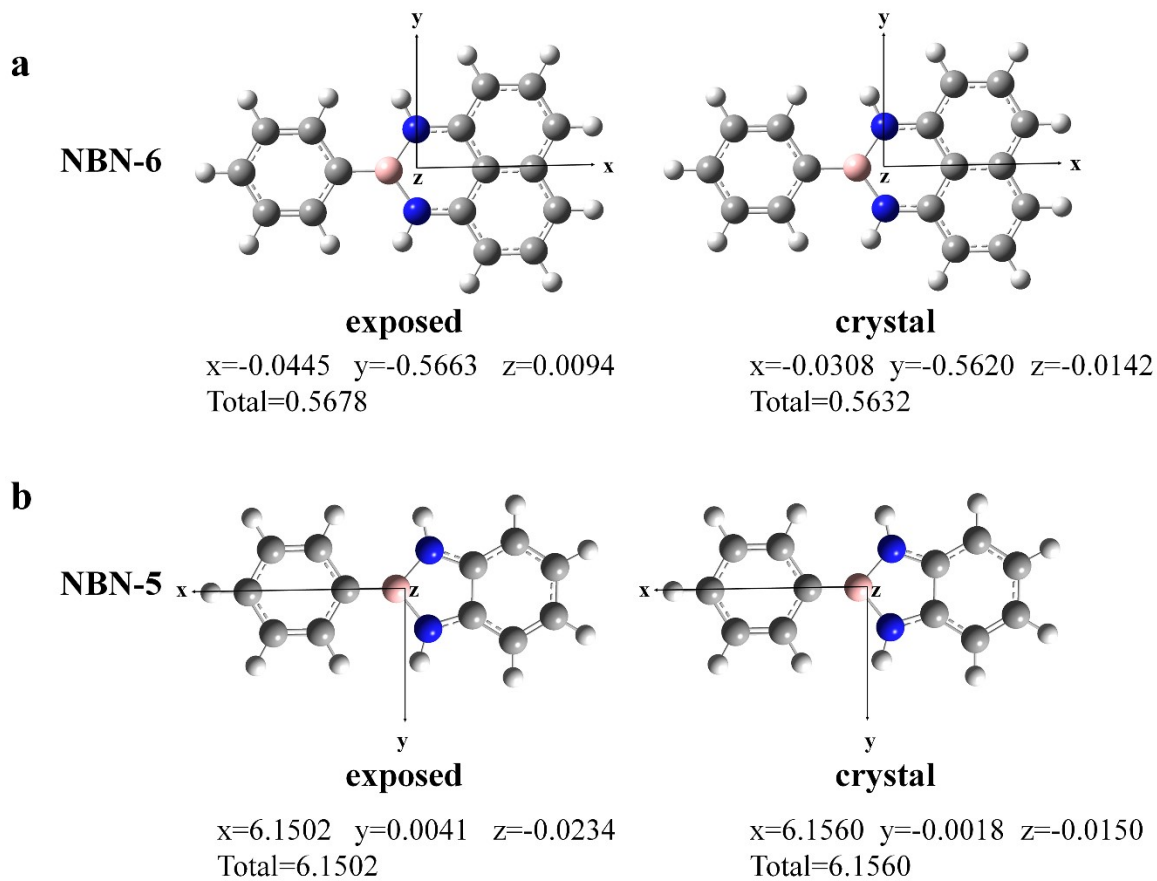


Fig. S9 Transition dipole moments of (a) NBN-6 and (b) NBN-5 at S_1 geometries of the exposed and crystalline phase. (units: Debye)

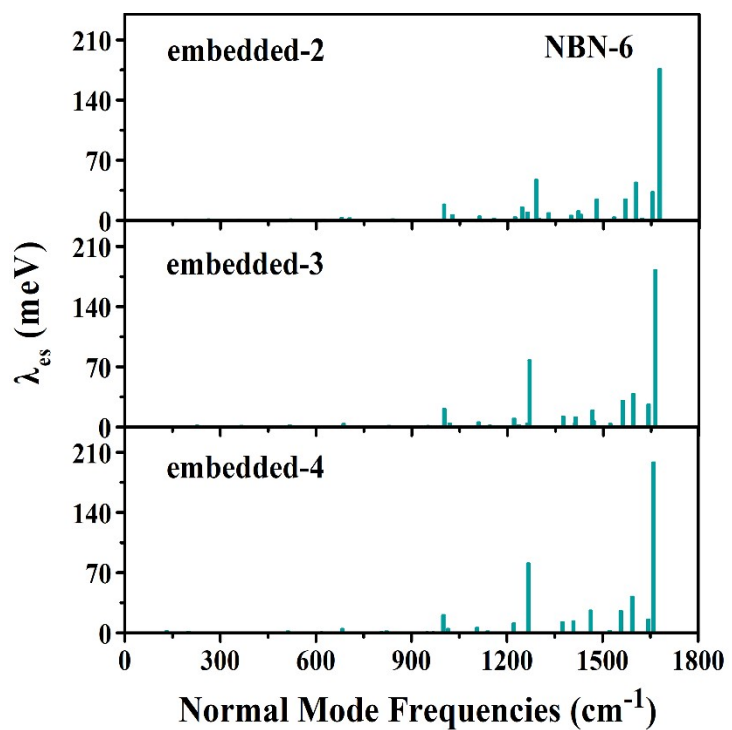


Fig. S10 Reorganization energy *vs* normal mode frequency of S_1 state of three representative embedded NBN-6 molecules in amorphous aggregates.

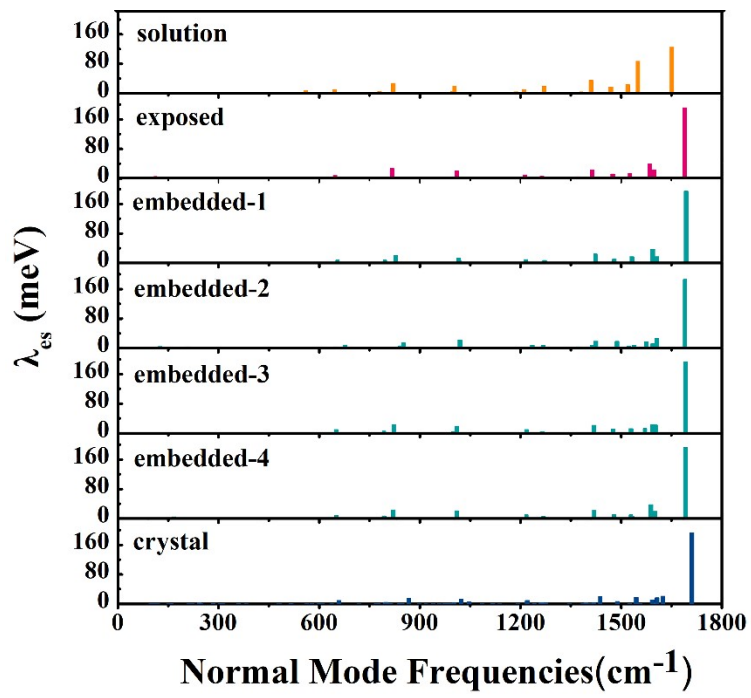
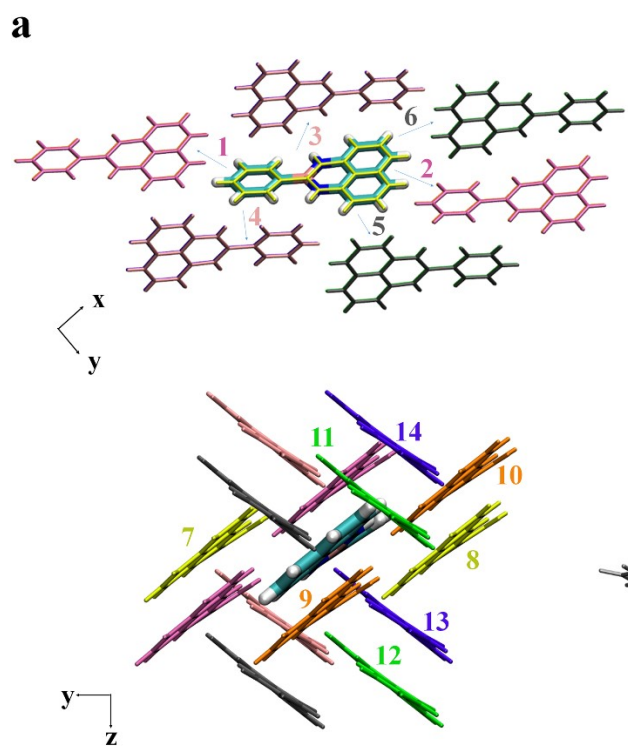


Fig. S11 Reorganization energy vs normal mode at S_1 state of NBN-5 molecules at different environments.

NBN-6



NBN-5

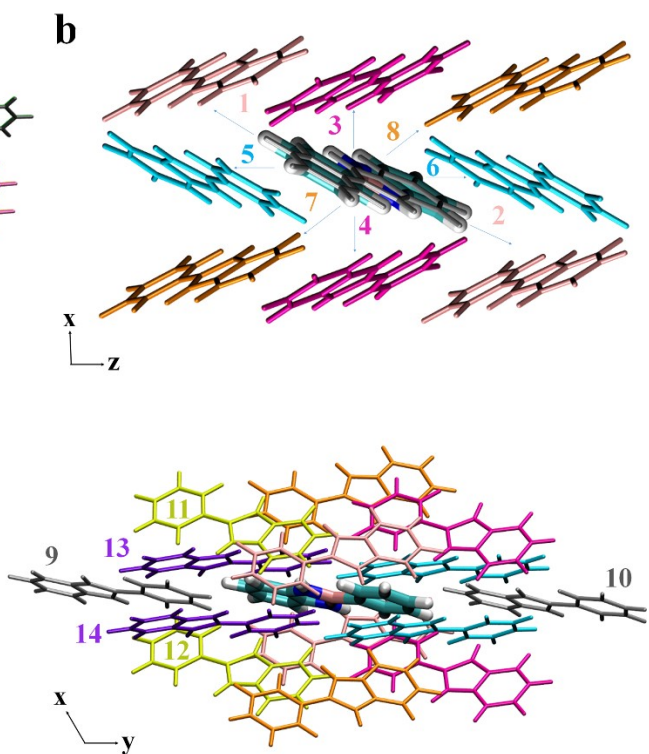


Fig. S12 The molecular packing in crystal along different directions of (a) NBN-6 and (b) NBN-5.

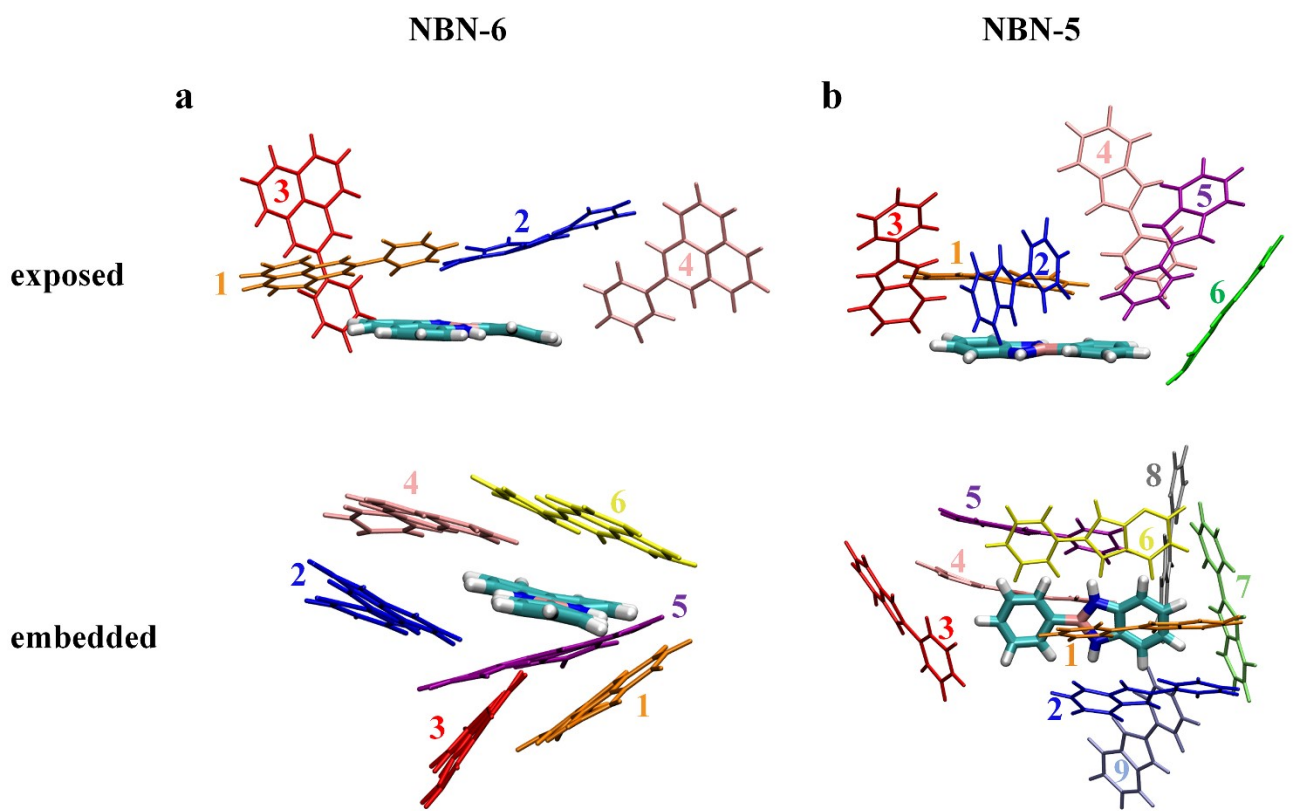


Fig. S13 The molecular packing around the selected QM molecule of (a) NBN-6 and (b) NBN-5 extracted from the amorphous aggregates.

III. Supplementary Tables

Table S1. The calculated absorption and emission wavelength, as well as excitation energies of NBN-6 and NBN-5 in methanol solution by PCM model using several different functionals with basis set 6-31+G(d,p), respectively.

	TPSSh	B3LYP	mPW1LYP	PW6B95	BMK	M06-2X	exper. ¹⁹
NBN-6	absorption 397 nm (3.12 eV)	370 nm (3.35 eV)	357 nm (3.47 eV)	354 nm (3.50 eV)	323 nm (3.84 eV)	320 nm (3.88 eV)	327 nm (3.79 eV)
	emission 526 nm (2.36 eV)	480 nm (2.58 eV)	454 nm (2.73 eV)	444 nm (2.79 eV)	388 nm (3.20 eV)	360 nm (3.44 eV)	462 nm (2.68 eV)
NBN-5	absorption 314 nm (3.95 eV)	302 nm (4.11 eV)	294 nm (4.22 eV)	288 nm (4.31 eV)	270 nm (4.59 eV)	268 nm (4.63 eV)	297 nm (4.18 eV)
	emission 388 nm (3.20 eV)	376 nm (3.30 eV)	367 nm (3.38 eV)	358 nm (3.46 eV)	334 nm (3.71 eV)	327 nm (3.79 eV)	387 nm (3.20 eV)

Table S2. Selected structural parameters of NBN-6 at different environments (including solution, one exposed and four embedded molecule of amorphous aggregates, crystal) at both S_0 and S_1 minimum, respectively.

NBN-6	solution			exposed			embedded-1			embedded-2			embedded-3			embedded-4			crystal	exper. ¹⁹			
	S_0	S_1	$ S_1-S_0 $	S_0	S_1	$ S_1-S_0 $	S_0	S_1	$ S_1-S_0 $	S_0	S_1	$ S_1-S_0 $	S_0	S_1	$ S_1-S_0 $	S_0	S_1	$ S_1-S_0 $	S_0	S_1	$ S_1-S_0 $		
C ₃ -B	1.57	1.50	0.07	1.57	1.49	0.08	1.57	1.49	0.08	1.57	1.49	0.08	1.57	1.49	0.08	1.56	1.48	0.08	1.57	1.49	0.08	1.56	
N ₁ -C ₁₀	1.40	1.35	0.05	1.40	1.34	0.06	1.40	1.34	0.06	1.40	1.34	0.06	1.40	1.34	0.06	1.39	1.34	0.05	1.40	1.34	0.05	1.40	
B-N ₁	1.43	1.48	0.05	1.43	1.48	0.05	1.42	1.48	0.06	1.43	1.49	0.06	1.43	1.49	0.06	1.42	1.48	0.06	1.42	1.48	0.06	1.41	
C ₃ -C ₄	1.41	1.45	0.04	1.41	1.45	0.04	1.41	1.45	0.04	1.41	1.45	0.04	1.41	1.45	0.04	1.41	1.44	0.03	1.41	1.44	0.04	1.39	
C ₄ -C ₅	1.40	1.38	0.02	1.40	1.45	0.05	1.39	1.38	0.01	1.39	1.38	0.01	1.40	1.38	0.02	1.39	1.38	0.01	1.39	1.38	0.01	1.38	
0₁	N₁-B-N₂	115.5	111.3	4.2	115.4	110.0	5.4	115.1	109.9	5.2	114.8	109.7	5.2	115.1	110.0	5.1	115.5	110.4	5.1	115.3	110.1	5.1	115.6
0₂	C₃-B-N₁	122.3	124.4	2.1	122.8	125.9	3.1	122.8	125.4	2.6	122.0	124.6	2.5	122.4	124.9	2.5	122.6	124.9	2.3	122.2	124.7	2.6	122.4
0₃	C₄-C₃-C₈	117.3	114.6	2.7	117.2	114.8	2.4	116.9	114.9	2.0	116.6	114.6	2.1	116.7	114.7	2.0	117.4	115.4	2.0	116.9	114.9	2.1	116.9
0₄	C₃-C₄-C₅	121.5	122.5	1.0	121.6	122.3	0.7	121.7	122.2	0.5	122.2	122.6	0.5	122.1	122.6	0.5	121.7	122.1	0.4	121.7	122.2	0.5	121.8
0₅	C₄-C₅-C₆	120.0	121.3	1.3	120.0	121.3	1.3	120.0	121.3	1.3	119.8	121.1	1.2	119.8	121.0	1.2	119.7	120.9	1.2	120.1	121.3	1.2	120.1
0₆	C₅-C₆-C₇	119.6	117.8	1.8	119.6	118.1	1.5	119.5	118.1	1.4	119.4	118.0	1.4	119.3	117.9	1.4	119.7	118.3	1.4	119.6	118.2	1.4	119.3
	C ₉ -C ₁₀ -N ₁	118.1	119.4	1.3	118.1	119.8	1.7	117.9	119.4	1.5	118.1	119.6	1.5	118.1	119.6	1.5	118.4	119.9	1.5	117.8	119.3	1.5	117.7
	C ₁₀ -C ₉ -C ₁₁	120.8	119.8	1.0	120.8	119.4	1.4	120.8	119.4	1.4	120.6	119.3	1.4	120.7	119.4	1.3	120.9	119.5	1.4	120.9	119.5	1.3	121.1
	B-N ₁ -H	121.0	119.5	1.5	121.1	118.2	2.9	120.7	117.8	2.9	121.4	118.4	2.9	121.3	118.2	3.1	121.8	118.7	3.1	121.0	118.0	3.0	119.1
D₁	C₄-C₃-B-N₁	153.0	180.0	27.0	158.7	174.7	16.0	173.4	177.0	3.6	173.9	179.0	5.1	174.9	178.1	3.2	179.2	179.7	0.5	171.5	175.4	3.9	172.2
	N ₁ -C ₁₀ -C ₁₂ -C ₁₄	179.9	180.0	0.1	178.0	177.2	0.8	173.9	173.9	0.0	178.4	177.5	0.8	178.1	178.5	0.4	179.3	179.6	0.3	179.5	179.4	0.1	179.3
	N ₂ -C ₁₁ -C ₁₃ -C ₁₅	179.9	180.0	0.1	179.4	179.9	0.5	178.1	178.2	0.1	178.7	179.5	0.8	179.1	179.6	0.5	174.5	172.9	1.6	179.7	179.7	0.0	179.7

Table S3. Selected structural parameters of NBN-5 at different environments (including solution, one exposed and four embedded molecule of amorphous aggregates, crystal) at both S_0 and S_1 minimum, respectively.

NBN-5		solution			exposed			embedded-1			embedded-2			embedded-3			embedded-4			crystal		exper.	
		S_0	S_1	$ S_1-S_0 $	S_0	S_1	$ S_1-S_0 $	S_0	S_1	$ S_1-S_0 $	S_0	S_1	$ S_1-S_0 $	S_0	S_1	$ S_1-S_0 $	S_0	S_1	$ S_1-S_0 $	S_0	S_1	$ S_1-S_0 $	
	C ₃ -B	1.56	1.49	0.07	1.56	1.49	0.07	1.56	1.49	0.07	1.56	1.49	0.07	1.56	1.49	0.07	1.56	1.49	0.07	1.55	1.48	0.07	1.55
	N ₁ -C ₉	1.39	1.35	0.04	1.40	1.35	0.05	1.39	1.35	0.04	1.39	1.35	0.04	1.39	1.35	0.04	1.40	1.35	0.05	1.38	1.35	0.03	1.38
	B-N ₁	1.44	1.50	0.06	1.44	1.50	0.06	1.44	1.50	0.06	1.43	1.48	0.05	1.44	1.50	0.06	1.44	1.50	0.06	1.43	1.49	0.06	1.44
	C ₃ -C ₄	1.41	1.45	0.04	1.41	1.45	0.04	1.41	1.44	0.03	1.40	1.43	0.03	1.41	1.44	0.03	1.41	1.45	0.04	1.4	1.44	0.04	1.41
	C ₄ -C ₅	1.40	1.38	0.02	1.39	1.38	0.01	1.39	1.38	0.01	1.40	1.38	0.02	1.40	1.38	0.02	1.39	1.38	0.01	1.39	1.37	0.02	1.40
0₁	N₁-B-N₂	104.7	101.4	3.3	104.5	101.2	3.3	104.6	101.3	3.3	104.1	100.7	3.4	104.6	101.3	3.3	104.7	101.4	3.3	103.8	100.6	3.2	104.6
0₂	C₃-B-N₁	127.7	129.3	1.6	128.0	129.5	1.5	127.0	128.3	1.3	123.0	124.1	1.1	126.1	127.4	1.3	128.3	129.8	1.5	126.6	128	1.4	126.4
0₃	C₄-C₃-C₈	117.3	115.5	1.8	117.1	116.1	1.0	117.2	116.2	1.0	116.9	115.8	1.1	117.3	116.4	0.9	117.3	116.3	1.0	117.3	116.3	1	117.7
0₄	C₃-C₄-C₅	121.6	121.9	0.3	121.7	121.6	0.1	121.7	121.7	0.0	122.1	122.4	0.3	121.5	121.5	0.0	121.7	121.6	0.1	121.6	121.7	0.1	121.4
0₅	C₄-C₅-C₆	120.0	121.1	1.1	120.0	120.8	0.8	119.7	120.6	0.9	119.8	120.4	0.6	120.0	120.7	0.7	119.9	120.7	0.8	119.8	120.6	0.8	119.7
0₆	C₅-C₆-C₇	119.6	118.5	1.1	119.6	118.9	0.7	119.9	119.3	0.6	119.5	118.8	0.7	119.7	119.1	0.6	119.6	118.9	0.7	120	119.4	0.6	120.1
	B-N ₁ -C ₉	109.6	110.8	1.2	109.7	110.9	1.2	109.6	110.8	1.2	110.8	112.0	1.2	109.8	110.9	1.1	109.6	110.7	1.1	110.4	111.6	1.2	109.7
	C ₁₀ -C ₉ -N ₁	108.1	108.5	0.4	108.0	108.5	0.5	108.0	108.4	0.4	107.5	107.8	0.2	108.1	108.5	0.4	108.0	108.4	0.4	107.6	107.9	0.3	107.9
	B-N ₁ -H	129.5	128.3	1.2	129.4	127.5	1.9	129.2	127.1	2.1	125.3	123.9	1.4	129.1	127.2	1.9	129.4	127.4	2.0	128.9	126.9	2.0	128.6
D₁	C₄-C₃-B-N₁	174.3	180.0	5.7	176.5	178.9	2.4	177.1	177.6	0.5	176.6	173.3	3.3	175.3	177.8	2.5	175.2	179.9	4.7	178.0	179.4	1.4	177.9
	B-N ₁ -C ₉ -C ₁₁	180.0	179.9	0.1	179.5	179.8	0.3	178.7	178.6	0.1	174.0	171.6	2.4	177.8	175.9	1.9	177.5	175.6	1.9	178.1	178.2	0.1	179.5

Table S4. The calculated NICS(1) values of ring A, B and C in NBN-6 and NBN-5.

NBN-6				NBN-5			
NICS(1)	ring A	ring B	ring C	NICS(1)	ring A	ring B	ring C
S ₀	-9.87	2.61	-8.45	S ₀	-9.45	-5.34	-10.23
T ₁	-0.02	-13.23	-3.57	T ₁	12.90	-4.72	-7.14

Table S5. Calculated vertical excitation energy (ΔE_{vert}), EDM, f and the transition orbitals assignment of NBN-6 and NBN-5 at the different phases.

		absorption				emission			
		ΔE_{vert}	EDM	f	assignments	ΔE_{vert}	EDM	f	assignments
NBN-6	solution	3.48 eV/ 356 nm	0.54 D	0.0014	HOMO→LUMO (90.1%)	2.73 eV/454 nm	0.73 D	0.0055	HOMO→LUMO (97.6%)
	exposed	3.37 eV/368 nm	0.04 D	0.0000	HOMO→LUMO (93.9%)	2.37 eV/523 nm	0.57 D	0.0029	HOMO→LUMO (98.2%)
	embedded-1	3.31 eV/375 nm	0.10 D	0.0001	HOMO→LUMO (94.9%)	2.37 eV/524 nm	0.57 D	0.0030	HOMO→LUMO (98.3%)
	embedded-2	3.30 eV/375 nm	0.10 D	0.0001	HOMO→LUMO (94.9%)	2.36 eV/526 nm	0.57 D	0.0029	HOMO→LUMO (98.3%)
	embedded-3	3.30 eV/375 nm	0.08 D	0.0001	HOMO→LUMO (94.8%)	2.36 eV/525 nm	0.57 D	0.0029	HOMO→LUMO (98.3%)
	embedded-4	3.29 eV/377 nm	0.08 D	0.0001	HOMO→LUMO (94.9%)	2.37 eV/523 nm	0.55 D	0.0029	HOMO→LUMO (98.3%)
	crystal	3.32 eV/374 nm	0.07 D	0.0001	HOMO→LUMO (94.6%)	2.38 eV/521 nm	0.56 D	0.0029	HOMO→LUMO (98.2%)
NBN-5	solution	4.23 eV/293 nm	7.15 D	0.5924	HOMO→LUMO (96.98%)	3.38 eV/367 nm	8.13 D	0.8417	HOMO→LUMO (98.89%)
	exposed	4.25 eV/ 292 nm	5.37 D	0.4636	HOMO→LUMO (96.95%)	3.35 eV/370 nm	6.01 D	0.4595	HOMO→LUMO (98.6%)
	embedded-1	4.26 eV/291 nm	5.37 D	0.4646	HOMO→LUMO (97.11%)	3.55 eV/350 nm	6.14 D	0.5077	HOMO→LUMO (99.02%)
	embedded-2	4.26 eV/291 nm	5.32 D	0.4568	HOMO→LUMO (97.01%)	3.52 eV/353 nm	6.02 D	0.4837	HOMO→LUMO (98.94%)
	embedded-3	4.25 eV/292 nm	5.38 D	0.4653	HOMO→LUMO (97.10%)	3.52 eV/352 nm	6.14 D	0.5034	HOMO→LUMO (99.02%)
	embedded-4	4.25 eV/292 nm	5.35 D	0.4619	HOMO→LUMO (96.94%)	3.52 eV/353 nm	6.11 D	0.4907	HOMO→LUMO (99.02%)
	crystal	4.23 eV/293 nm	5.43 D	0.4721	HOMO→LUMO (97.17%)	3.54 eV/351 nm	6.16 D	0.5089	HOMO→LUMO (98.96%)

Table S6. Contributions of heavy atoms in rings B and C to HOMO and LUMO of both NBN-6 and NBN-5.

	NBN-6		NBN-5	
	HOMO	LUMO	HOMO	LUMO
B (p _z)	0	0.162	B (p _z)	0.085
N (p _z)	0.091	0.025	N (p _z)	0.087
N (p _z)	0.091	0.025	N (p _z)	0.087
C ₉ (p _z)	0	0.029	C ₉ (p _z)	0.162
C ₁₀ (p _z)	0.066	0.005	C ₁₀ (p _z)	0.162
C ₁₁ (p _z)	0.066	0.005	C ₁₁ (p _z)	0.018
C ₁₂ (p _z)	0.137	0.003	C ₁₂ (p _z)	0.018
C ₁₃ (p _z)	0.137	0.003	C ₁₃ (p _z)	0.135
C ₁₄ (p _z)	0.026	0.002	C ₁₄ (p _z)	0.135
C ₁₅ (p _z)	0.026	0.002	Total	0.889
C ₁₆ (p _z)	0.178	0.009		
C ₁₇ (p _z)	0.178	0.009		
C ₁₈ (p _z)	0	0		
Total	0.996	0.279		

Table S7. Calculated k_r , k_{ic} and fluorescent quantum efficiency (FQE) of both NBN-6 and NBN-5 at different environments (including methanol solution, exposed and embedded molecules in amorphous aggregates and crystals).

	NBN-6			NBN-5		
	k_r (10^5 s $^{-1}$)	k_{ic} (10^7 s $^{-1}$)	FQE %	k_r (10^8 s $^{-1}$)	k_{ic} (10^7 s $^{-1}$)	FQE%
solution	7.4	15000	0.0005	4.2	2.1	95.2
exposed	7.1	470	0.02	2.2	0.48	97.9
embedded-1	7.3	5.6	1.3	2.8	1.0	96.5
embedded-2	7.0	5.9	1.2	2.6	0.32	98.8
embedded-3	7.0	5.9	1.2	2.7	1.1	96.1
embedded-4	7.1	4.6	1.5	2.6	0.35	98.7
crystal	7.1	3.8	1.8	2.8	0.14	99.5

Table S8. Reorganization energies of NBN-6 and NBN-5 obtained by both the adiabatic potential energy surface (AP) and normal mode analysis (NM) methods in the different phases.

		AP			NM		
	meV	λ_{gs}	λ_{es}	λ_{total}	λ_{gs}	λ_{es}	λ_{total}
NBN-6	solution	352	396	748	1184	1656	2840
	exposed	501	497	998	507	730	1237
	embedded-1	483	456	939	479	479	958
	embedded-2	488	456	944	485	480	965
	embedded-3	484	456	940	481	480	961
	embedded-4	478	444	922	476	467	943
NBN-5	crystal	477	459	936	476	479	955
	solution	370	479	849	362	401	763
	exposed	357	368	725	355	398	753
	embedded-1	331	384	715	354	385	739
	embedded-2	364	376	740	374	392	766
	embedded-3	359	363	722	360	385	745
	embedded-4	366	368	734	365	394	759
	crystal	339	358	697	347	372	719

Table S9. The projected reorganization energies of six representative normal modes of NBN-6 at different environments.

NBN-6	exposed		embedded		crystal	
mode ID	frequency (cm ⁻¹)	λ (meV)	frequency (cm ⁻¹)	λ (meV)	frequency (cm ⁻¹)	λ (meV)
Mode 1	96	44.36	104	0.69	115	0.01
Mode 2	98	14.96	118	1.01	122	3.38
Mode 3	996	29.38	998	20.74	1002	22.45
Mode 4	1017	40.63	1015	5.82	1024	3.13
Mode 5	1226	46.03	1221	9.60	1229	11.25
Mode 6	1271	101.21	1267	75.57	1268	77.02

Table S10. The excitonic coupling constants (J) of pairwise dimers (shown in Fig. S11) extracted from the crystal structures of NBN-6 and NBN-5.

Molecule ID	NBN-6		NBN-5	
	Distance (Å)	J (meV)	Distance (Å)	J (meV)
1	11.8099	0.300	6.9294	35.020
2	12.9984	0.143	6.9829	30.585
3	5.4972	0.470	6.9366	4.243
4	8.1395	0.052	6.9366	4.243
5	8.2260	1.967	7.8845	6.063
6	12.4263	0.056	8.1054	10.351
7	5.4299	0.212	6.9829	30.585
8	5.4299	0.212	6.9294	35.020
9	12.9984	0.143	10.7514	15.056
10	11.8099	0.300	10.7514	15.056
11	12.4263	0.056	6.0398	32.689
12	8.2260	1.967	6.0398	32.689
13	8.1395	0.052	8.1054	10.351
14	5.4972	0.470	7.8845	6.063

Table S11. The excitonic coupling constants (J) of pairwise dimers (shown in Fig. S12) extracted from the amorphous aggregates of NBN-6 and NBN-5.

		NBN-6		NBN5	
	Molecule ID	Distance (Å)	J (meV)	Distance (Å)	J (meV)
exposed	1	7.387	1.8	4.349	34.3
	2	6.722	0.3	6.599	13.1
	3	9.517	0.4	11.879	12.0
	4	12.557	0.0	8.975	22.9
	5			9.351	19.6
	6			9.855	18.8
embedded	1	4.454	0.7	5.821	34.3
	2	7.518	1.9	5.561	33.5
	3	7.118	0.1	10.061	22.0
	4	6.729	1.1	6.180	19.5
	5	8.613	1.2	5.576	22.6
	6	9.672	1.2	6.140	36.2
	7			7.675	5.1
	8			8.455	22.2
	9			9.220	23.5

Table S12. Intermolecular distances for the dimer with the maximum excitonic coupling constants (J) at different environments and the corresponding ratios J/λ_{gs} and J/λ_{es} of NBN-6 and NBN-5.

		Distance (Å)	J (meV)	λ_{gs} (meV)	λ_{es} (meV)	J/λ_{gs}	J/λ_{es}
NBN-6	exposed	7.387	1.8	501	497	0.004	0.004
	embedded-1	7.518	1.9	483	456	0.004	0.004
	embedded-2	4.800	1.7	488	456	0.003	0.004
	embedded-3	4.925	3.2	484	456	0.007	0.007
	embedded-4	3.852	2.7	478	444	0.006	0.006
NBN-5	crystal	8.226	2.0	476	479	0.004	0.004
	exposed	4.349	34.3	357	368	0.096	0.093
	embedded-1	6.140	36.2	331	384	0.109	0.094
	embedded-2	4.331	35.2	364	376	0.096	0.093
	embedded-3	10.352	21.6	359	363	0.048	0.048
	embedded-4	9.765	26.0	366	368	0.071	0.071
	crystal	6.930	35.0	339	358	0.103	0.098

IV. References

1. Z. Chen, C. S. Wannere, C. Corminboeuf, R. Puchta and P. v. R. Schleyer, *Chem. Rev.*, 2005, **105**, 3842-3888.
2. P. v. R. Schleyer, C. Maerker, A. Dransfeld, H. Jiao and N. J. R. van Eikema Hommes, *J. Am. Chem. Soc.*, 1996, **118**, 6317-6318.
3. Z. Chen, C. S. Wannere, C. Corminboeuf, R. Puchta and P. Schleyer, *Chem. Rev.*, 2005, **105**, 3842-3888.
4. H. Fallah-Bagher-Shaidei, C. S. Wannere, C. Corminboeuf, R. Puchta and P. v. R. Schleyer, *Org. Lett.*, 2006, **8**, 863-866.
5. C. Lee, W. Yang and R. G. Parr, *Phys. Rev. B*, 1988, **37**, 785-789.
6. C. Adamo and V. Barone, *J. Chem. Phys.*, 1998, **108**, 664-675.
7. J. R. Cheeseman, G. W. Trucks, T. A. Keith and M. J. Frisch, *J. Chem. Phys.*, 1996, **104**, 5497-5509.
8. K. Wolinski, J. F. Hinton and P. Pulay, *J. Am. Chem. Soc.*, 1990, **112**, 8251-8260.
9. J. Gauss, *J. Chem. Phys.*, 1993, **99**, 3629-3643.
10. R. McWeeny, *Phys. Rev.*, 1962, **126**, 1028-1034.
11. H. B. S. G. W. T. M. J. Frisch, G. E. Scuseria, M. A. Robb, J. R. Cheeseman, G. Scalmani, V. Barone, G. A. Petersson, H. Nakatsuji, X. Li, M. Caricato, A. V. Marenich, J. Bloino, B. G. Janesko, R. Gomperts, B. Mennucci, H. P. Hratchian, J. V. Ortiz, A. F. Izmaylov, J. L. Sonnenberg, D. Williams-Young, F. Ding, F. Lipparini, F. Egidi, J. Goings, B. Peng, A. Petrone, T. Henderson, D. Ranasinghe, V. G. Zakrzewski, J. Gao, N. Rega, G. Zheng, W. Liang, M. Hada, M. Ehara, K. Toyota, R. Fukuda, J. Hasegawa, M. Ishida, T. Nakajima, Y. Honda, O. Kitao, H. Nakai, T. Vreven, K. Throssell, J. A. Montgomery, Jr., J. E. Peralta, F. Ogliaro, M. J. Bearpark, J. J. Heyd, E. N. Brothers, K. N. Kudin, V. N. Staroverov, T. A. Keith, R. Kobayashi, J. Normand, K. Raghavachari, A. P. Rendell, J. C. Burant, S. S. Iyengar, J. Tomasi, M. Cossi, J. M. Millam, M. Klene, C. Adamo, R. Cammi, J. W. Ochterski, R. L. Martin, K. Morokuma, O. Farkas, J. B. Foresman, and D. J. Fox., Gaussian16 Revision A.03. Gaussian Inc. Wallingford CT, 2016.
12. D. Geuenich, K. Hess, F. Köhler and R. Herges, *Chem. Rev.*, 2005, **105**, 3758-3772.
13. T. A. Keith and R. F. W. Bader, *Chem. Phys. Lett.*, 1992, **194**, 1-8.
14. T. A. Keith and R. F. W. Bader, *Chem. Phys. Lett.*, 1993, **210**, 223-231.
15. F. Plasser, *J. Chem. Phys.*, 2020, **152**, 084108.
16. F. Plasser, M. Wormit and A. Dreuw, *J. Chem. Phys.*, 2014, **141**, 024106.
17. F. Plasser and H. Lischka, *J. Chem. Theory Comput.*, 2012, **8**, 2777-2789.
18. W. Humphrey, A. Dalke and K. Schulten, *J. Mol. Graph. Model.*, 1996, **14**, 33-38.
19. W. Wan, D. Tian, Y. Jing, X. Zhang, W. Wu, H. Ren and H. Bao, *Angew. Chem., Int. Ed.*, 2018, **57**, 15510-15516.